DESIGN AND EXPERIMENT OF AUTOMATIC STRIP-ZONING PESTICIDE APPLICATION CONTROL SYSTEM FOR SOYBEAN-MAIZE STRIP INTERCROPPING BASED ON MACHINE VISION
/
基于机器视觉的大豆玉米带状复合种植自动分带施药控制系统设计与试验

Gongpei CUI, Huanhuan CHEN, Yu ZHANG, Zishang YANG, Lele WANG, He LI *)
College of Mechanical and Electrical Engineering, Henan Agricultural University, Zhengzhou, Henan, China
Tel: +86 15515549801; E-mail: lihenjx@henau.edu.cn
Corresponding author: He Li
DOI: https://doi.org/10.35633/inmateh-79-35

Keywords: *soybean-maize strip intercropping; machine vision; peak method; ROI; precision zoning; least squares method*

ABSTRACT
The soybean-maize strip intercropping mode has been widely popularized, yet existing plant protection machinery fails to dynamically adjust pesticide application according to crop zones, suffers from poor pesticide application accuracy, and is prone to causing crop damage. Aiming at the above problems, this study proposed a precise strip-zoning pesticide application method for soybean and maize and established an automatic strip-zoning pesticide application control system based on machine vision. Perspective transformation was adopted to correct image viewing angles; after subsequent processing via excess green binarization and opening-closing operations, a dynamic ROI (Region of Interest) positioning and recognition algorithm for crop rows based on the peak value method was applied. The least square method was used to extract crop row lines, the offset was calculated according to the geometric relationship of the centerlines of soybean and maize zones, and an automatic strip-zoning offset compensation model was constructed to achieve precise strip-zoning. Field experiment results show that: under conditions with little shadow and stable light, the recognition algorithm achieved the optimal performance with an accuracy of up to 92%. At operating speeds of 2–5 km/h, the automatic strip-zoning pesticide application control system had a mean strip-zoning deviation of ≤3.16 cm, with the proportion of deviations within 5 cm reaching 84% (up to 94%). Under wind speeds of 1.4–2.9 m/s, the maximum droplet drift deposition amount of the closed anti-drift device was 9.41 droplets per cm², delivering favorable strip-zoning pesticide application performance, which provides data support and a reference for field precision plant protection operations under the strip intercropping mode.

摘 要
大豆玉米带状复合种植模式广泛推广，但现有植保机械无法随作物带进行动态调整施药，且施药精度差，易造成伤害。针对上述问题，本文基于机器视觉，提出一种大豆玉米精准分带施药方法并搭建自动分带施药控制系统。采用透视变换校正图像视角，再经超绿二值化与开闭运算处理后，基于峰值法的作物行动态 ROI（Region of interesting）定位识别算法，采用最小二乘法提取作物行线，依据大豆玉米带中心线的几何关系计算偏移量并构建自动分带偏移补偿模型以实现精准分带。田间试验结果表明：在阴影少、光照稳定条件下，识别算法效果最佳，准确率可达 92%。自动分带施药控制系统在 2-5km/h 的速度下分带偏差均值≤3.16cm，5cm 内偏差占比达 84%（最高 94%）。1.4m/s~2.9m/s 风速条件下，封闭式防飘移装置的雾滴飘移沉积量最高为 9.41 个/cm2，具有较好的分带效果，为复合种植模式下的田间精准植保作业提供数据支撑与参考。

INTRODUCTION
Soybean and maize are important food crops, and efficient and precise plant protection operations constitute a key measure to improve their yield *(Cui et al., 2023; Zhang et al., 2025)*. At present, the mainstream pesticide application equipment for the soybean-maize strip intercropping mode is the traditional fixed zoned boom sprayer *(Khan et al., 2024; Zhang et al., 2024)*. Although it can realize zoned pesticide application to a certain extent, it is unable to perceive the dynamic information of field crop zones and achieve precise pesticide application when confronted with problems such as inconsistent inter-zone spacing and irregular sowing rows in the sowing process. Therefore, there is an urgent need to develop a technical scheme for field precision plant protection adapted to this cropping mode.

At present, scholars at home and abroad have carried out extensive research in the field of precision control such as crop row line extraction. *Zhao et al., (2016),* proposed an operation line extraction method suitable for wheat harvesting, which adopted the cross-correlation function method to detect the boundary points between the harvested area and the to-be-harvested area, and fitted the target line via the Hough transform. *Chen et al., (2019)* mapped the fitting straight lines obtained from different accumulation thresholds of the Hough transform to the parameter space, clustered the parameter space data by K-means clustering, and regarded the cluster centroids in the parameter space under the optimal accumulation threshold as the identified actual crop rows. *Chen et al., (2020)* adopted a median point Hough transform based on an optical system for navigation line fitting, which was 24 ms faster than the traditional Hough transform. In addition, *Yang et al., (2020),* used the least square method to obtain navigation lines in the dynamic ROI area on the basis of static ROI, with a recognition accuracy of 96%. *Liao. et al., (2019),* counted the pixel points of crop rows by sub-region and took them as candidate feature points, retained valid feature points based on the distance threshold, and performed straight line fitting on the feature points using the least square method, with an extraction accuracy of 95.6%. *Hossein et al., (2014),* extracted crop row center lines using the Hough transform and centroid image processing algorithm respectively, with the average time consumption of the two algorithms being 0.7 s and 0.4 s. *Montalvo et al., (2012),* proposed a crop row detection method based on the moving window method for maize fields with high weed density, which was superior to the traditional Hough transform in processing efficiency. However, the above methods are restricted by factors such as application scenarios and algorithm time consumption, and their robustness and accuracy need to be further improved. Meanwhile, all these studies are conducted for homogeneous crops, leading to poor applicability.

Aiming at the above problems, this study established an automatic strip-zoning pesticide application control system and proposed a dynamic ROI positioning and recognition algorithm for crop rows based on the peak value method, which fused perspective transformation, vertical projection, strip segmentation and the least square method for crop row fitting. Meanwhile, the offset was calculated according to the geometric relationship of the centerlines of soybean and maize zones, and an offset compensation model was constructed. The traditional PID control algorithm was introduced to enhance the regulation capability of the actuation output of the automatic strip-zoning pesticide application control system, thereby enabling rapid response and correction of deviations caused by changes in the field environment. Finally, the system was deployed on a strip-type boom sprayer to conduct field performance experiments. The results show that the recognition algorithm has a certain robustness under different light conditions. At different operating speeds, the system can effectively perform strip-zoning pesticide application and reduce crop phytotoxicity, which holds certain practical significance for strip-zoning pesticide application under the strip intercropping mode.

MATERIALS AND METHODS

1. Automatic Strip-zoning Pesticide Application Control System for Soybean-maize Intercropping Based on Machine Vision

1.1 Structural Composition of the Automatic Strip-zoning Pesticide Application Control System

The overall structure of the automatic strip-zoning boom sprayer for pesticide application based on machine vision is shown in Fig. 1, which is mainly composed of a power system, travel assembly, image acquisition and processing module, strip-zoning control module, and soybean-maize pesticide application module. The sprayer has a wheel base of 1.8 m and is powered by a single-cylinder diesel engine with a rated power of 14.7 kW, which can meet the requirements of normal field operations for the automatic strip-zoning pesticide application control system.

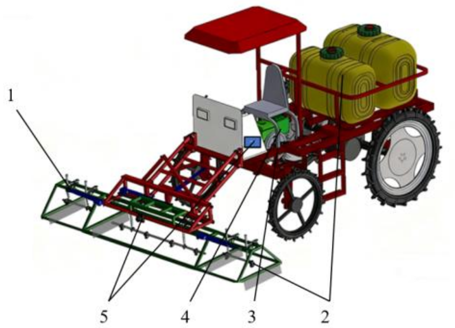

Fig. 1 - Structural Schematic Diagram of Automatic Strip-zoning Boom Sprayer

1 - Lateral adjustment spray boom mechanism; 2 - Soybean-maize pesticide application module; 3 - Travel assembly; 4 - Power system; 5 - Image acquisition and processing module

The structure of the automatic strip-zoning pesticide application control system is mainly composed of a lateral adjustment spray boom mechanism, a control unit and an image acquisition and processing module. Among them, the lateral adjustment spray boom mechanism consists of a middle spray boom frame, side spray boom frames and a lifting mechanism. One end of the central electric push rod is fixed to the lifting bracket, and the other end is connected to the middle spray boom frame. The sliders are arranged between the slide rails and the middle spray boom frame, and the two side spray boom frames are in sliding contact with the middle spray boom frame respectively, with a maximum operating width of 4.2 m. The control unit is mainly composed of a Delta PLC (Programmable Logic Controller), a Leadshine driver and a stepping push rod motor; the stepping push rod motor has a maximum stroke of 0.5 m and a maximum telescopic speed of 0.2 m/s. For the image acquisition and processing module, the acquisition device is an LT-USB 1080P depth camera (Lantian Technology Co., Ltd.), with a frame rate of 30 frames per second and a maximum video image resolution of 1920×1080. It is equipped with a 2.8–16 mm zoom lens and installed at a height of 1200 mm, which can effectively cover the target crop area. The built-in computer is configured with an Intel Core i5 processor, 16 GB of ROM, 512 GB of storage and 8 GB of RAM, which can basically meet the field operation requirements.

1.2 Working Principle of the Automatic Strip-zoning Pesticide Application Control System

As shown in Fig. 2, during field operation, the field crop row information (RGB images) collected by the LT-USB 1080P depth camera is transmitted to the upper computer via USB. The upper computer software calculates the lateral offset of the boom in real time and transmits it to the lower computer controller (PLC) through the RS485 serial port. The lower computer controller controls the left and right movement of the push rod motor via the Leadshine driver, and the Oedila rope displacement sensor feeds back the telescopic length of the push rod motor to the lower computer controller in real time, thereby achieving precise control of the boom's movement position. A speed sensor (E6B2-CWZ6C1000P incremental encoder, Omron Corporation) collects the operating speed of the sprayer in real time.

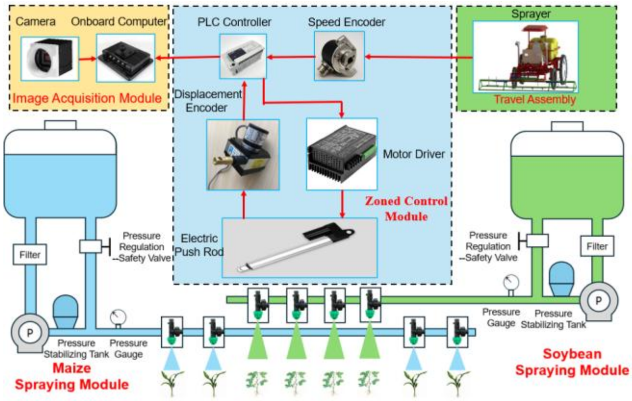

Fig. 2 - Flow Chart of Working Principle of Automatic Strip-Zoning Pesticide Application Control System

2. Recognition Method of Crop Zone Row Line Based on Machine Vision

Recognition of crop zone row lines is a prerequisite for achieving precision strip-zoning pesticide application. This paper adopts the peak value method for the fitting of soybean and maize crop zone row lines, and the specific process is illustrated in Fig. 3.

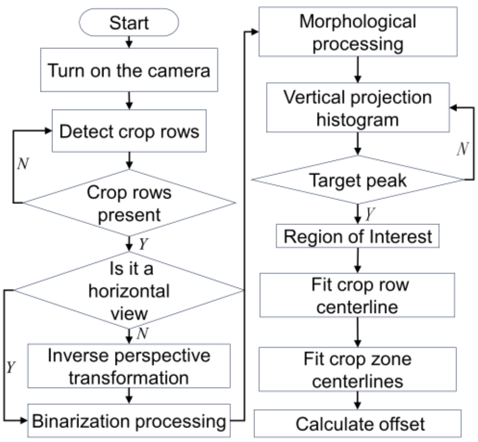

Fig. 3 - Flow Chart of Crop Zone Centerline Fitting

2.1 Image Acquisition and Preprocessing

2.1.1 Image Acquisition

Images were captured in a soybean-maize strip intercropping test field in Xinzheng City, Henan Province, with the shooting conducted from May to June 2025. The camera was mounted at a height of 1200 mm with an inclination angle of 30°. For subsequent research and analysis, soybean-maize videos with a resolution of 1280×720 pixels under different light conditions were selected, as shown in Fig. 4(a).

2.1.2 Image Preprocessing

2.1.2.1 Inverse Perspective Transformation

To maintain clear, parallel and equally wide boundaries of soybean and maize rows, effectively segment different crop zones, and avoid zonal segmentation errors caused by the convergence and overlap of distant crop zones in crop images, inverse perspective transformation was performed on the collected images *(Li et al., 2024; Tang et al., 2018; Zhao et al., 2019 ; Zhang et al., 2023)*.

As shown in Fig. 4, during plant protection operations, on the premise that the machine operates at a constant speed in a straight line while the camera angle and image size remain unchanged, four sets of valid pixel coordinates were selected from the image containing the target crop rows to form the boundary for inverse perspective transformation, and the target region was extracted accordingly. The inverse perspective transformation from Fig. 4(b) to Fig. 4(d) can be realized by means of the homography matrix (H matrix). From the transformation results, the crop rows are arranged in parallel without converging to infinity. This method can effectively reduce the computational complexity of the subsequent algorithm and facilitate the follow-up crop row line fitting *(Khan et al., 2024)*.

$$x' = H.x \tag{1}$$

where: H is the 3×3 homography matrix; x' is the corresponding plane coordinates in the transformed image, [Pixel]; x is the corresponding plane coordinates in the original image, [Pixel].

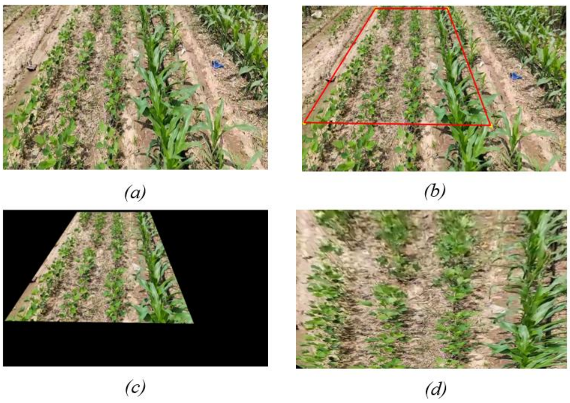

Fig. 4 - Inverse Perspective Transformation

(a) Original image; (b) Region division; (c) Region of Interest; (d) Perspective transformation

2.1.2.2 Image Segmentation

Segmenting crop regions from complex backgrounds such as soil and weeds is crucial for improving algorithm efficiency and achieving precision strip-zoning. Currently, image segmentation algorithms are mainly categorized into three types: color index-based segmentation, threshold-based segmentation, and deep learning-based segmentation *(Guerrero et al., 2013; Sun et al., 2022; Pérez-Ruíz et al., 2014; Jiang et al., 2014)*.

On this basis, this paper selected three typical segmentation algorithms, and ultimately determined the one with the optimal performance by comparing the time consumption and segmentation effectiveness of single-channel grayscale images under different climatic conditions.

(1) The VARI (Vegetation Index)-based image segmentation algorithm is mainly used to identify green vegetation regions from RGB images. Its core lies in utilizing the characteristic that the green component (*G*) is significantly higher than the red component (*R*), and reducing the impact of illumination intensity variations through normalization processing. The algorithm is presented as follows.

$$\begin{cases} VARI = (G - R) / D & (-1,1) \\ D = G + R - B & D \neq 0 \end{cases} \tag{2}$$

Based on this algorithm, green feature extraction was performed on the images, and the binarized images were further optimized via morphological operations, as shown in Fig. 5(b).

(2) An image preprocessing method based on the HSV color space. By adjusting the threshold ranges of hue, saturation and value, i.e., setting the values of the H, S and V channels within the green threshold range, the pixel values of green crops are enhanced while the non-green background is suppressed. To achieve effective segmentation of crop plants from the background, this paper combines the H and S channels: the green regions are filtered out by adjusting the threshold of the H channel, the S channel of the green regions is retained, and grayscale conversion is performed subsequently. The processing results are shown in Fig. 5(c).

(3) $2G\text{-}R\text{-}B$ based on the Excess Green Index is a green feature enhancement algorithm rooted in the RGB color space. It strengthens the weight of the green component and suppresses the red and blue components simultaneously, which makes the green regions more prominent after processing and facilitates subsequent segmentation and feature extraction. Its grayscale image is shown in Fig. 5(d).

$$ExG = 2G - R - B \tag{3}$$

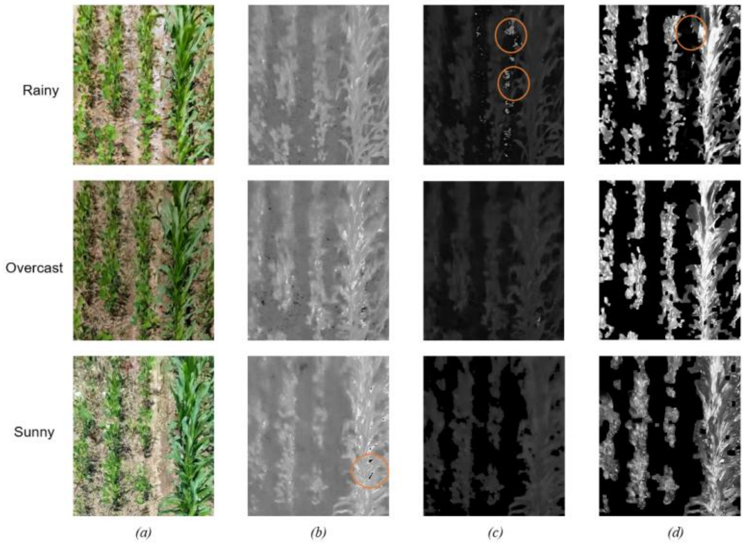

Fig. 5 - Grayscale Image Effect Comparison

(a) Original image; (b) VARI grayscale image; (c) HSV grayscale image; (d) 2G-R-B grayscale image

As shown in Fig. 5, a comparative analysis of the segmentation performance of the three different algorithms revealed that VARI could completely segment crops from the background under all three weather conditions, yet the resulting images were blurry with a time consumption of 201 ms. In comparison with the Excess Green algorithm, HSV leads to target loss and was prone to noise in rainy weather, which interfered with subsequent binarization processing. By contrast, the Excess Green-based segmentation algorithm could well preserve green crops; the time consumption of the Excess Green algorithm was 109 ms and that of the HSV algorithm is 98 ms. Considering the segmentation performance, time consumption and post-processing requirements comprehensively, the Excess Green algorithm was adopted as the preprocessing segmentation algorithm in this study. In view of the enhanced processing of green features by the Excess Green algorithm, to better constrain the range of green regions, this paper adopted the HSV threshold method in color space binarization for binarization processing, and the corresponding binary mask was generated by setting the threshold ranges of each HSV channel.

The expression is presented as follows.

$$\begin{cases} hsv\text{-}low = (H_{min},\ \ S_{min},\ \ V_{min}) \\ hsv\text{-}high = (H_{max},\ \ S_{max},\ \ V_{max}) \end{cases} \tag{4}$$

After completing the segmentation of the image foreground and background, there still exist noise and holes caused by interfering factors such as dew and shadows. These defects impair the image segmentation performance and hinder the subsequent detection of crop rows. In this study, morphological processing involving a closing operation followed by an opening operation was applied to the images, which can effectively fill gaps, eliminate noise, reduce interference from irrelevant detailed information, and enhance the algorithm's adaptability to complex environments.

Fig. 6 illustrates the corresponding processes of grayscale conversion, binarization and morphological processing.

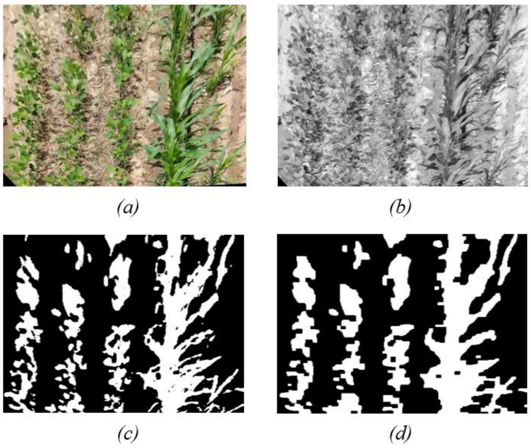

Fig. 6 - Binarization Processing Effect
(a) Original; (b) Grayscale; (c) Binarized; (d) Morphologically processed

2.2. Extraction of the Crop Zone Centerline

After acquiring the crop canopy characteristics, further post-processing is required for the preprocessed images to fit the geometric centerlines of the crop row canopy, laying a solid foundation for the extraction of the crop zone centerline.

2.2.1. Adaptive ROI Acquisition

The research object of this study is the test field under the soybean-maize strip intercropping mode. To achieve precision strip-zoning pesticide application, the recognition targets should be focused on the inter-zone areas between soybean zones and maize zones. In view of the complex field environment under the intercropping mode, which is likely to impair the algorithm recognition accuracy, this study adopts the peak value method to demarcate the ROI for the purpose of reducing interference from non-recognition areas *(Ota et al., 2022; Ramesh et al., 2016; Zhang et al., 2023)*. Given the known width (Width) and height (Height) of the preprocessed images, the expression for vertical projection is as follows:

$$S(j)=\sum_{i=1}^{H}P(i,j) \tag{5}$$

where: (i,j) is the pixel coordinates of the vertical projection, [Pixel]; $P(i,j)$ is the target pixel coordinates, [Pixel]; $S(j)$ is the cumulative value of target pixels in the $j\text{-}th$ column, [Pixel].

Images are susceptible to noise caused by factors such as illumination and soil. To prevent minor wave crests from interfering with the subsequent identification of peak points, this study adopted mean filtering to perform denoising processing on the images.

Fig. 7 - Vertical Projection Filtering Effect
(a) Before filtering; (b) After filtering

As shown in Fig. 7, four white vertical projections correspond to the position information of the four crop rows. Statistics of the cumulative pixel values and inspection of each contour are carried out on the vertical projection histogram. A height threshold T_k is set, which can filter out minor noise peaks. In this study, the height threshold is determined based on the mean value plus the standard deviation of the projection data.

Let the mean value be denoted as μ and the standard deviation as σ. The mean value represents the average value of each pixel array in the vertical projection, and the standard deviation characterizes the degree of dispersion of the array. In the vertical projection, the total pixel value of the "Target Peaks" (the columns corresponding to crop rows) is inevitably higher than the background mean value, while "noise" refers to random values that fluctuate slightly around the mean value. To obtain an optimal height threshold, 1σ and 2σ are selected to achieve a balance between the risk of peak missing and anti-noise capability. The expression is given as follows.

$$\mu+1\sigma\le T_k\le\mu+2\sigma \tag{6}$$

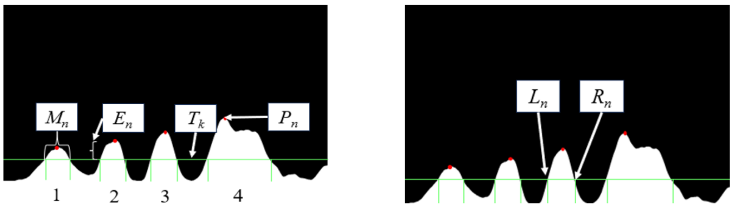

Fig. 8 - Algorithm Processing Effect

The research object of this study is limited to the adjacent vertical projection contours of soybean and maize, and valid contours are filtered out based on the global peak difference and peak width difference, for which the following expression is derived:

$$P_n = S(j)_{max} \tag{7}$$

where: $S(j)_{max}$ is the maximum cumulative value of target pixels, [Pixel].

Compare the M_n values of each contour from 1 to 4 and select the maximum value, then calculate the peak difference with its adjacent contour. The contour with the largest difference is retained to obtain the target contour, which narrows the ROI. To acquire complete crop rows, the peak values of the two contours are taken as reference points, with one target width ($\bar{M}$) expanded to the left and right respectively. The expression is as follows:

$$\bar{M} = \frac{1}{k}\sum_{i=1}^{n} M_i \tag{8}$$

where: k is the coefficient (related to crop growth conditions); n is the number of contours, which is known to be 2.

Analysis of program operation reveals that the value range of k is [2, 5]. The k value was screened using 200 images: different k coefficients were adopted with an increase step of 1, and the crop row retention effect was observed, from which it was concluded that k=3 meets the requirements. The positioning effect of the first ROI is shown in Fig. 9(a).

To extract the crop zone centerline and reduce the computational load of the recognition algorithm, a second ROI demarcation is performed for the soybean and maize row regions. On the basis of the first ROI, the rising edge boundaries and falling edge boundaries of the vertical projection contours of the soybean seedling rows and maize seedling rows were searched for and recorded. The ROI region was identified by acquiring the known height threshold T_k and boundary positioning points, as shown in Fig. 9(b).

Fig. 9 - ROI Localization Effect

(a) First ROI; (b) Second ROI

2.2.2. Crop Zone Centerline Fitting

As the core reference benchmark for an agricultural machinery vision plant protection system to complete offset detection and compensation, the crop zone centerline can clearly distinguish the spatial boundaries and central positions of soybean zones and maize zones, provide accurate displacement control commands for the automatic strip-zoning pesticide application control system, and ensure that operating components such as the spray boom and nozzles are accurately aligned with the crop zones. Its fitting process is illustrated in the figure below:

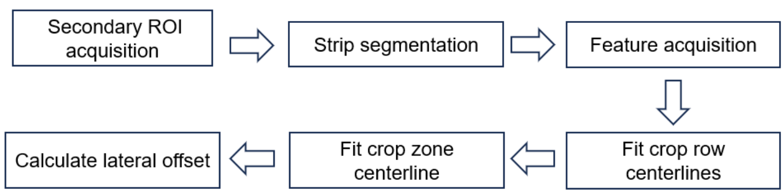

Fig. 10 - Flow Chart of The Crop zone Centerline Extraction

Strip segmentation was carried out on the basis of the second ROI. To reduce the computational load, the number of strips is set to N, and N is taken as 10 in this study. Vertical projection processing is performed on the pixels within each strip. Given the width W and height H of the ROI, the height of each strip is denoted by the mathematical expression ΔH. The mathematical expressions for the strips are given as follows.

$$S(j) = \sum_{i=1}^{\Delta H} P(i, j) \tag{9}$$

In the preprocessed images, the higher the leaf area ratio in the column direction, the larger the value of $S(j)$. The algorithm traverses $S(j)$ of each strip from left to right, excludes the values lower than the threshold, identifies the first and last qualified columns, and takes their average value to obtain the feature point ($\Delta H/2$, j). Subsequently, it traverses downward with a step size of ΔH within the ROI, collecting the feature points until all horizontal strips are completely traversed. The performance of the algorithm is shown in Fig. 11.

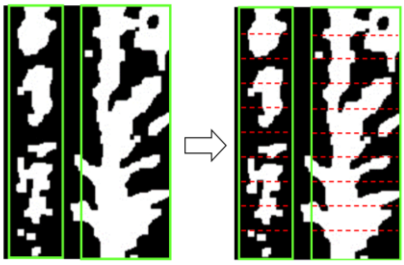

Fig. 11 - Strip Segmentation Effect

The crop row feature points obtained from each of the aforementioned strips are stored in a point set, and the fitting of the centerlines of soybean rows and maize rows is achieved based on the Least Squares Method *(Liao et al., 2019; McInnes et al., 2017; Ota et al., 2022; Vidovic et al., 2016; Yang et al., 2022)*. Ultimately, the crop zone centerline is derived by virtue of *the Parallel Centerline Principle*, with the results shown in Fig. 12.

Fig. 12 - Extraction Results of the Crop Zone Centerline

3. Realization of Offset Compensation Model and Strip-Zoning Control

3.1. Offset Calculation

3.1.1. Coordinate System Transformation

Coordinate System Transformation is a prerequisite for calculating the actual offset information of crop rows. To convert the identified row position information in the image into the actual displacement data in the world coordinate system, it is necessary to perform camera calibration and eliminate the errors caused by camera distortion.

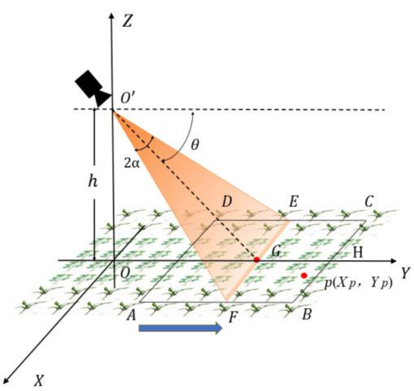

Fig. 13 - Geometric Relationship of the Camera Field of View in the World Coordinate System

As shown in Fig. 13, $ABCD$ in the figure represents the field of view (FOV) of the camera on the ground, point O' denotes the camera optical center, and point O is the projection coordinate of the camera on the ground, which also serves as the origin of the world coordinate system. Point P is the actual ground coordinate point corresponding to a pixel point p on the image, with the coordinate of (X_p,Y_p). G is the intersection point of the optical axis and the ground. The resolution of the industrial camera is $m\times n$, 2β is the vertical field of view angle ($\angle HO'O$), and 2α is the horizontal field of view angle ($\angle EO'F$). The calculation formulas are as follows:

$$\beta = arctan(\frac{Vc}{2f}) \tag{10}$$

$$\alpha = arctan(\frac{Vc'}{2f}) \tag{11}$$

where: β represents the half the vertical field of view angle, [°]; α represents the half the horizontal field of view angle, [°]; V_c is the sensor height, [mm]; V_c' is the sensor width, [mm].

From the camera sensor parameters, V_c is 2.92 mm, V_c' is 5.18 mm and f is 3.6 mm, from which β is calculated as 22.07 ° and α as 35.75 °.

Given a camera installation angle of 30°, the depression angle θ of the camera can be calculated as follows:

$$\theta = 30^\circ + \beta \tag{12}$$

θ is calculated as 52.07 °.

From the deduction based on the inverse perspective mapping formula, the corresponding coordinates of pixel point p in the world coordinate system can be obtained. Its expression is given as follows:

$$u = \frac{mY_p - htan\theta}{2Y_p tan\theta tan\alpha + 2htan\alpha} \tag{13}$$

$$v = \frac{nX_p}{2tan\alpha\sqrt{h^2+Y_p^2}}\sqrt{1+\left(\frac{2utan\beta}{m}\right)^2} \tag{14}$$

where: u is the x-coordinate of point p on the image plane, [Pixel]; v is the y-coordinate of point p on the image plane, [Pixel].

Four coordinate systems are involved in the image processing process, namely the image coordinate system UO_0V, the image physical coordinate system XOY, the camera coordinate system $X_cO_cY_c$, and the world coordinate system $X_wO_wY_w$, as shown in Fig.15. The transformation relationship between the coordinates of any point in the image coordinate system and its corresponding coordinates in the world coordinate system is as follows:

$$\mathbf{Z}_c\begin{bmatrix}u\\v\\1\end{bmatrix} = \begin{bmatrix}\frac{f}{dx} & 0 & 0 & 0\\ 0 & \frac{f}{dy} & 0 & 0\\ 0 & 0 & 1 & 0\end{bmatrix}\begin{bmatrix}R & T\\ 0 & 1\end{bmatrix}\begin{bmatrix}X_w\\Y_w\\Z_w\\1\end{bmatrix} = M_1M_2\begin{bmatrix}X_w\\Y_w\\Z_w\\1\end{bmatrix} \tag{15}$$

where: O_w-$X_wY_wZ_w$ is the world coordinate system, used to describe the camera position, [m]; O_c-$X_cY_cZ_c$ is the camera coordinate system, with the optical center as the origin, [m]; o-xy is the image coordinate system, with the midpoint of the imaging plane as the origin, [mm]; p is the point in the world coordinate system, i.e., a real physical point in the actual scene, [mm]; (u,v) are the coordinates of point p in the pixel coordinate system, [Pixel]; (x,y) are the coordinates of point p in the image coordinate system, [Pixel]; M_1 is the intrinsic parameter matrix ; M_2 is the extrinsic parameter matrix, which contains the rotation matrix R and the translation matrix T ; f is the camera focal length, i.e., [mm]. the distance between o and Oc, as shown in Fig. 14.

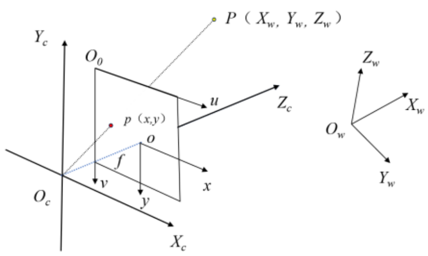

Fig. 14 - Schematic Diagram of Coordinate System Transformation

Two camera calibration methods based on OpenCV and MATLAB are currently available: the former is susceptible to image quality with relatively large calibration errors, while the latter requires manual extraction of corner points and features high accuracy with low calibration error. This study adopted the MATLAB-based calibration method: the calibration toolbox was invoked via the calib_gui command to import 20 calibration images, the checkerboard used had a square side length of 20 mm, and the results of corner point extraction are shown in Fig. 15.

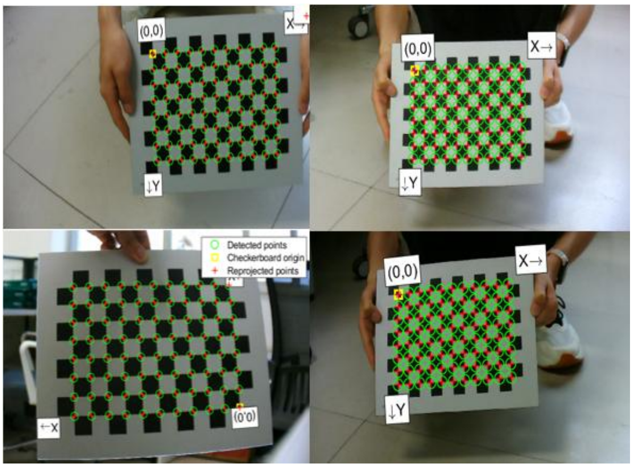

Fig. 15 - Corner Point Extraction Effect of the Calibration Board

As shown in Table 1 are the intrinsic and extrinsic parameter matrices of the target camera obtained via the MATLAB calibration toolbox.

Table 1

Camera Calibration Results

Property	Parameter
K	[763.1029,0,0;0,762.2424,0;629.5229,345.8421,1]
Radial Distortion	[0.130846983244061, -0.150301138293976]
Tangential Distortion	[0,0]

3.1.2. Lateral Offset Compensation Control Variable

To achieve precise strip-zoning spraying, it is necessary to calculate the offset information of the crop zone centerline. The linear distance in the horizontal direction from the calibrated nozzle fixed on the anti-drift baffle to the crop zone centerline is defined as the offset. In the offset compensation model shown in Fig. 16(a), Zones 1 and 2 are the blind areas of the camera's field of view, among which Zone 1 refers to the area corresponding to the distance from the nozzle to the camera, and Zone 3 is the camera's field of view area. The crop zone centerline l: $Ax+By+C=0$ is derived from the soybean row centerline l_1: $Ax+By+C_1=0$ and the maize row centerline l_2: $Ax+By+C_2=0$ in accordance with the Parallel Centerline Principle. The point (x_0, y_0) represents the relative coordinate of a point on the crop zone centerline within Zone 3 with respect to the absolute coordinate system O, and ΔE denotes the actual lateral distance from this point to the nozzle, as given by the following formula:

$$\Delta E = \frac{|Ax_0 + By_0 + C|}{\sqrt{A^2 + B^2}} \tag{16}$$

The installation position coordinates and mounting angle of the industrial camera are shown in Fig. 16. The nozzle is fixed on the spray boom frame, and the actual distance L_1 from point (x_0, y_0) to the nozzle is jointly composed of y_0, L_2 and L_3, which can be expressed as:

$$\begin{cases} L_1 = y_0 + L \\ L = L_3 + L_2 \\ L_3 = h \tan \lambda \end{cases} \tag{17}$$

where: λ is the included angle between the lower boundary plane of the camera's field of view and the vertical direction, [°]; L_2 is the straight-line distance between the nozzle and the camera, [m]; L_3 is the straight-line distance between the camera and the field of view boundary, [m].

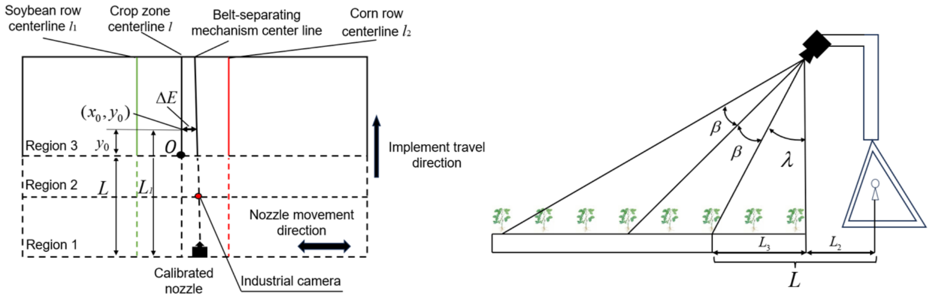

(a) (b)

Fig. 16 - Schematic Diagram of the Offset Compensation Model

(a) Top View; (b) Side View

When the automatic strip-zoning pesticide application control mechanism receives the execution signal, it cannot act immediately, and speed regulation control is thus required. The speed sensor mounted on the wheels captures the operating speed v_1, from which the safety boundary of the delayed execution time for the strip-zoning control system, t_1, is derived.

$$t_1 \leq \frac{L_1}{v_1} \tag{18}$$

Only when the time taken for the sprayer to operate a distance L satisfies the safety boundary condition can the row alignment mechanism complete the compensation for the offset ΔE. On this basis, an offset compensation model is established, yielding the response speed of the strip-zoning control mechanism as follows:

$$v_2 = \frac{\Delta E}{t_1} \tag{19}$$

To optimize the dynamic response characteristics of the offset compensation system, a position closed-loop control scheme based on a PD trajectory tracking strategy with PID control is designed in accordance with the established kinematic model of the row alignment mechanism (Fig. 16). This scheme is intended to significantly improve the response speed and accuracy of the system during target trajectory tracking by optimizing the controller design *(Ding et al., 2019; Han et al., 2022; Zheng et al., 2023)*. The expression is given as follows:

$$O_{pd} = K_p r + K_d \Delta r_0 + K_i \sum_{n=0}^{k} \Delta r_n \tag{20}$$

where: O_{pd} is the pulse output frequency, [Hz]; K_p is the proportional coefficient; K_d is the differential coefficient; K_i is the integral coefficient; Δr is the offset error, [mm]; Δr_0 is the offset error at the previous moment, [mm]; $\sum_{n=0}^{k} \Delta r_n$ is the cumulative offset error, [mm].

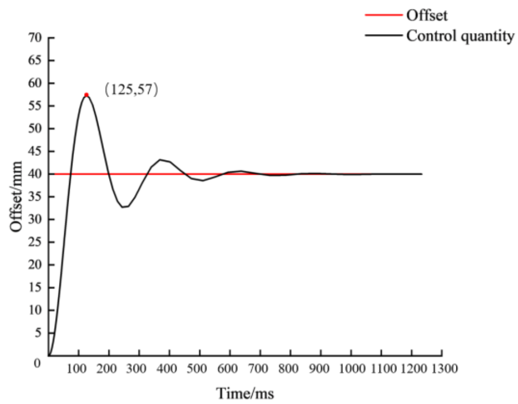

Fig. 17 - PD Control Curve

The results are shown in Fig. 17. When the target value was set to 40 mm, the maximum deviation of PD control reached 57 mm with a response time of 125 ms. To reduce the oscillation and instability phenomena occurring during the error adjustment process and enable the response speed of the actuator to be rapidly improved in a short time, the proportional coefficient K_p was determined as 2 and the differential coefficient K_d as 15 through manual tuning.

4 Experiment metrics and Determination Methods

4.1 Experiment metrics

This study selected the following core indicators to evaluate the system performance: mean recognition deviation and recognition accuracy reflect the recognition precision of the algorithm; mean deviation and the proportion of deviations within 50 mm reflect the strip-zoning accuracy of the system; droplet deposition density verifies the effect of strip-zoning pesticide application. The expressions are as follows:

$$\mu = \frac{1}{N}\sum_{i=1}^{N} x_i \tag{21}$$

$$P = \frac{N_{correct}}{N_{total}} \times 100\% \tag{22}$$

$$D = \frac{N_C}{S_T} \tag{23}$$

where: μ is the mean value of recognition deviation; $N_{correct}$ is the Number of correctly identified samples; N_{total} is the Total number of identified samples; D is the droplet deposition density, [droplet/cm²]; N_C is the number of droplets collected by the water-sensitive paper, [droplet]; S_T is the area of the water-sensitive test paper, [cm²].

4.2 Determination Methods

To verify the various performance metrics of the automatic strip-zoning pesticide application control system, the experiment was conducted in a soybean-maize strip intercropping test field in Xinzheng City, Henan Province (*34.3791°N, 113.6489°E*).

For the performance measurement of the recognition algorithm, light detection software was used to acquire field light intensity information at different time periods throughout the day, and videos of crop rows were collected and subjected to frame segmentation. The algorithm recognition system was applied to measure recognition deviations, with deviations exceeding 5 cm defined as recognition errors (*Wang, Q. et al., 2021; García et al., 2017*).

In the experiments for the system and droplet anti-drift performance, as is shown in Fig. 18, a strip intercropping plant protection sprayer was adopted, and the automatic strip-zoning pesticide application control system was mounted on the boom sprayer. A speed sensor was installed inside the sprayer's wheels, and a rope displacement sensor was fitted on the spray boom to measure the offset of the actuator. An industrial camera was installed at the front of the sprayer and positioned at the mid-stroke of the electric push rod. A calibrated nozzle was fixed inside the anti-drift device directly below the industrial camera to record the trajectory of the droplet strip. A rectangular area with a length of 20 m and a width equal to the inter-zone spacing was demarcated in the crop zone area; within this area, a piece of water-sensitive paper and a warning line of the same length as the area were laid every 40 cm as reference benchmarks. Meanwhile, water-sensitive test paper was laid on the canopies of soybean and maize plants (Fig. 22). During the experiment, the operating speed of the plant protection sprayer was controlled at 2 km/h, 3 km/h, 4 km/h and 5 km/h. After the system received control commands, the nozzles sprayed uniformly, and the droplet positions were visualized by utilizing the characteristic of water-sensitive paper turning red upon contact with water. The experiment wind speed was measured at 1.4–2.9 m/s. Upon completion of the experiment, the coordinate positions of droplet centers on the water-sensitive paper were manually recorded, and the number of blue spots on the surface of the water-sensitive test paper was counted to verify the overall performance of the automatic strip-zoning pesticide application control system.

Fig. 18 - Field Experiment

RESULTS

5. Field Experiment and Analysis

5.1. Performance Experiment of the Recognition Algorithm

To verify the robustness of the algorithm's recognition performance, this study conducted performance tests under different light intensities, with the mean recognition deviation and recognition accuracy adopted for evaluation.

The experimental results are shown in Table 2. The algorithm's recognition performance is dependent on light intensity: during the period of 14:30–16:30, the light was uniform and stable without direct strong light or shadow occlusion, and the crop row recognition accuracy reached the peak of the entire experiment period under both forward and backlighting conditions. The distinct crop-background feature boundaries facilitated target segmentation and contour extraction; during 9:30–14:30, the light intensity rose to the maximum, and local overexposure of images led to the loss of texture features in crop canopies and a decrease in the contrast between targets and the background, resulting in an increase in the mean recognition deviation and a subsequent decline in accuracy; during 16:30–18:30, the light intensity diminished, the area of shadows from crop canopies and the machine expanded with a complex distribution, and blurred pixel features caused a reduction in positioning accuracy, with the mean recognition deviation reaching 3.53 cm, which was significantly higher than that in the previous two periods. Overall, the recognition accuracy of the algorithm remained above 84% throughout the entire experiment period, indicating a certain level of its adaptability to the field environment.

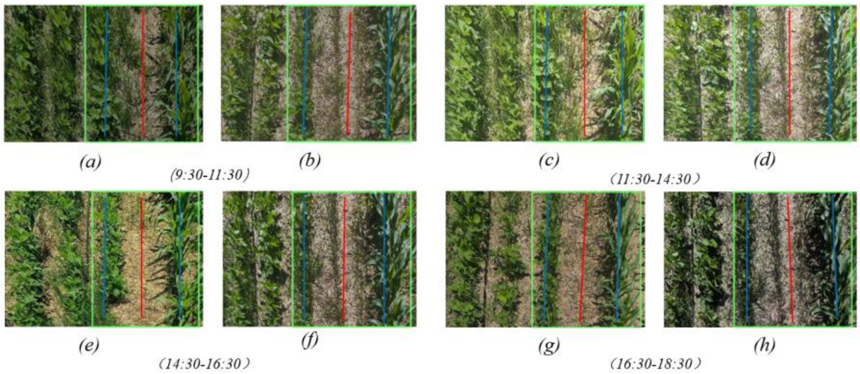

Fig. 19 - Light intensity experiment results

(a), (c), (e), (g)-- Frontlight; (b), (d), (f), (h)-- Backlight

Table 2

Light intensity experiment results

Time Interval	Light Intensity / Lux	Light Direction	Mean Recognition Deviation / cm	Recognition Accuracy / %
9:30-11:30	**1.66×10^4**	Frontlight	3.34	88
		Backlight	3.37	90
11:30-14:30	**1.79×10^4**	Frontlight	3.44	88
		Backlight	3.36	91
14:30-16:30	**1.39×10^4**	Frontlight	3.00	90
		Backlight	3.32	92
16:30-18:30	**1.15×10^4**	Frontlight	3.53	86
		Backlight	3.46	84

5.2. System Performance Experiment

To quantitatively analyze the real-time response characteristics of the visual recognition module and the automatic strip-zoning actuation mechanism, 20 groups of continuous and typically representative sample data were selected in this study while the sprayer was operating at an operating speed of 2 km/h, and the Trend Chart of Vision-Actuation Offset Variation (Fig. 20) was plotted accordingly.

As can be seen from Fig. 20, the strip-zoning actuation offset generally exhibits the characteristic of converging toward the visual recognition detection results. When the sprayer operated to Zone I, the crops grew uniformly with a reasonable planting density, and the crop row contours were clear and highly continuous. The automatic strip-zoning actuation mechanism featured a small displacement adjustment range and a rapid response, which reduced the offset to the minimum value of 0.3 cm throughout the entire operation process.

In contrast, when the sprayer operated to Zone II, the offset exhibited significant abnormal fluctuations, with the maximum offset reaching 4.9 cm, which was significantly higher than that in other operating areas.

This was due to the crop seedling absence in this zone, which led to the weakening of crop row contour features and the breakage of their continuity. This prevented the system's visual recognition module from accurately capturing the complete position of the crop zone centerline, which in turn caused a lag in the displacement adjustment of the automatic strip-zoning actuation mechanism and ultimately resulted in an increase in the offset.

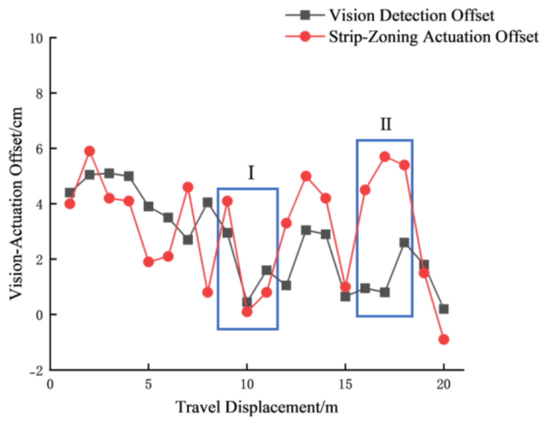

Fig. 20 - Trend Chart of Vision-Actuation Offset Variation

Meanwhile, the experiment set different operated speed gradients, and 50 groups of valid samples were selected for each gradient to plot the dynamic trend chart of the offset between the droplet zone center and the crop zone centerline (Fig. 21).

It can be seen from the trend characteristics in Fig. 21 that the offset exhibited a significant positive correlation with the increase in operating speed. The statistical characteristics of the crop zone trajectory offset under different speed gradients are shown in Table 3. Under the four operating speeds, the mean maximum deviation of the trajectory offset was all controlled within 50 mm. Among them, the mean offset fluctuated sharply at speeds of 2–4 km/h, with a maximum difference of 0.98 cm between adjacent speeds.

The main reasons are as follows: First, the nozzle and the boom frame are connected via a hinged joint. During the operating of the sprayer, the nozzle is prone to irregular lateral oscillation due to the unevenness of the field road surface and the inertial effect of the machine, which causes the droplet spray landing points to deviate from the preset area. Second, with the increase in the sprayer's operating speed, the video images collected by the system's visual recognition module suffer from insufficient resolution, which results in blurred boundary features between crop zones and a significant decline in contour recognizability. This makes it impossible to accurately extract the spatial position information of the inter-zone centerline, and thus the strip-zoning control actuation mechanism lacks a reliable visual perception basis for generating accurate offset compensation commands. This ultimately leads to continuous error accumulation, resulting in an obvious increasing trend of the mean offset with the rise in operating speed.

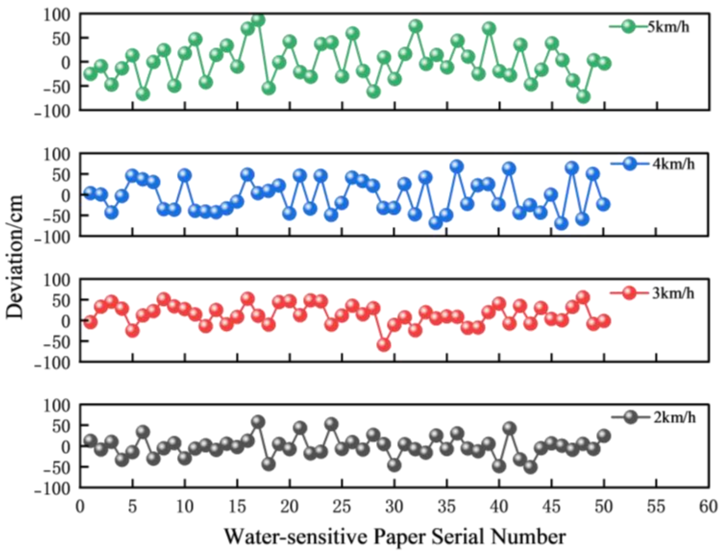

Fig. 21 - Deviation at Different Speeds

Table 3

Crop Strip Trajectory Deviation Statistics

Speed / km·h⁻¹	Mean Deviation / cm	Proportion of Deviations Within 50 mm / %
2	1.83	94.00
3	2.81	92.00
4	3.55	88.00
5	3.56	84.00

5.3 Drift Prevention Performance Experiment of Droplets

To further evaluate the strip-zoning effect of the automatic strip-zoning pesticide application control system, droplet cross-zone drift prevention performance experiment were conducted.

By calculating the droplet deposition density (Eq. 23), the deposition status of droplets per unit crop area can be determined *(Ma et al., 2023; Ni et al., 2020; Zhou et al., 2021)*. The results are shown in Tables 4 and 5.

Fig. 22 - Water-Sensitive Test Paper

Table 4

Maize Liquid Droplet Drift Deposition

Speed / km/h	Droplet Deposition Amount / (droplet /cm²)			Mean Droplet Deposition Amount / (droplet /cm²)
	1	2	3	
2	0.20	0.24	0.11	0.18
3	0.44	0.66	1.19	0.76
4	1.69	1.61	1.71	1.67
5	6.38	4.81	6.65	5.94

Table 5

Soybean Liquid Droplet Drift Deposition

Speed / km/h	Droplet Deposition Amount / (droplet /cm²)			Mean Droplet Deposition Amount / (droplet /cm²)
	1	2	3	
2	0.55	0.41	0.76	0.57
3	1.65	1.27	1.67	1.53
4	1.92	1.83	2.78	2.18
5	8.78	10.29	9.17	9.41

From the experimental results, the amount of droplet cross-zone drift is positively proportional to the operating speed, and the drift deposition amount of droplets is no more than 9.41 cm², which indicates that the system can effectively reduce droplet cross-zone drift.

CONCLUSIONS

(1) Taking soybean and maize under the strip intercropping mode as the research object, a crop row recognition algorithm and a strip-zoning spray control system were designed, and a vision-based strip-zoning pesticide application control system was established.

(2) Research is conducted on the crop row recognition method based on machine vision. A dynamic ROI positioning and crop row line extraction algorithm for soybean and maize crop rows based on the peak value method was proposed, and a strip-zoning offset compensation model was constructed accordingly.

(3) Field experiment results show that the light intensity at different times of the day causes slight fluctuations in the algorithm's recognition accuracy, while the recognition accuracy remains no less than 87% consistently. At operating speeds of 2 to 5 km/h, the mean strip-zoning deviation of the automatic strip-zoning pesticide application control system can be controlled within 3.61 cm, and the proportion of strip-zoning deviations within 5 cm reaches 84%, with a maximum of 94%. Under wind speeds of 1.4 to 2.9 m/s, the droplet drift deposition amount of the closed anti-drift device is directly proportional to the operating speed, with a maximum of 9.41 number/cm², which meets the plant protection operation standards for the soybean-maize strip intercropping mode. This study provides a practical technical reference for the development of precise plant protection operations under the soybean-maize intercropping mode.

ACKNOWLEDGEMENT

This work was supported by the Special Support Fund for High-level Talents of Henan Agricultural University (30501381), the Henan Provincial Science and Technology Commissioner Project (30804295), and the Henan Provincial Science and Technology Research and Development Program (242102111175).

REFERENCES

[1] Chen Z. W., Li W., Zhang W. Q., Li Y. W., Li M. S., Li H., (2019). Research on vegetable crop row extraction method based on automatic Hough transform accumulation threshold (基于自动 Hough 变换累加阈值的蔬菜作物行提取方法研究), *Transactions of the Chinese Society of Agricultural Engineering*, vol.35, no.22, pp.314-322, Chongqing/China. DOI: 10.11975/j.issn.1002-6819.2019.22.037

[2] Cui G. P., Sun X. J., Liu J. W., Shi Y. H., Li J. Y., Li Y. Q., Yu C. C., Cheng S. S., Li H., (2023). Design and test of strip-divided boom sprayer for soybean and corn strip compound planting (大豆玉米带状复合种植分带式喷杆喷雾机设计与试验), *Journal of Henan Agricultural University*, vol.57, no.5, pp.752-763, Zhengzhou/China. DOI:10.16445/j. cnki.1000-2340.20230828.001

[3] Ding Y. C., He Z. B., Xia Z. Z., Peng J. Y., Wu T. H., (2019). Design of immune PID controller for navigation of small crawler rapeseed seeder (小型履带式油菜播种机导航免疫 PID 控制器设计), *Transactions of the Chinese Society of Agricultural Engineering*, vol.35, no.7, pp.12-20, Wuhan/China. DOI: 10.11975/j.issn.1002-6819.2019.07.002

[4] García-Santillán I., Guerrero J., Montalvo M., Pajares G., (2017). Curved and straight crop row detection by accumulation of green pixels from images in maize fields, *Precision Agriculture*, vol.19, pp.18–41, Spain. DOI:10.1007/s11119-016-9494-1

[5] Jiang G. Q., Wang Z. H., Liu H. M., (2014). Automatic detection of crop rows based on multi-ROIs, *Computers and Electronics in Agriculture*, vol.42, no.5, pp.2429–2441, Jiaozuo/China. DOI: 10.1016/j.compag.2014.10.033

[6] Khan M. N., Rahi A., Rajendran V. P., Al Hasan M., Anwar S., (2024). Real-time crop row detection using computer vision-application in agricultural robots, *Frontiers in Artificial Intelligence*, vol.7, Article ID 1435686, IN/USA. DOI:10.3389/frai.2024.1435686

[7] Liao J., Wang Y., Yin J. N., Zhang S., Liu L., Zhu D. Q., (2019). Seedling row center line extraction based on sub-regional feature point clustering (基于分区域特征点聚类的秧苗行中心线提取), *Transactions of the Chinese Society for Agricultural Machinery*, vol.50, no.11, pp.34-41, Hefei/China. DOI: 10.6041/j.issn.1000-1298.2019.11.004

[8] Li Y. F., Wright B., Ha M. R. Z., (2024). Deep learning-based perspective distortion correction for outdoor photovoltaic module images, *Solar Energy Materials and Solar Cells*, vol.277, Article ID 113107, Sydney/Australia. DOI: 10.1016/j.solmat.2024.113107

[9] Ma K., Zhang Z. Y., Dong X. Y., Qiu B. J., (2023). Design and test of portable droplet deposition detection system (便携式雾滴沉积检测系统的设计与试验), *Journal of Agricultural Mechanization Research*, vol.45, no.5, pp.49-54, Zhenjiang/China. DOI: 10.13427/j.cnki.njyi.2023.05.045

[10] McInnes L., Healy J., Astels S., (2017). Hdbscan: hierarchical density based clustering, *Journal of Open Source Software*, vol.2, Article ID 205, Canada. DOI:10.21105/joss.00205.

[11] Montalvo M., Pajares G., Guerrero J. M., et al., (2012). Automatic detection of crop rows in maize fields with high weeds pressure, *Expert Systems with Applications*, vol.39, no.15, pp.11889–11897, Madrid/Spain. DOI:10.1016/j.eswa.2012.05.065

[12] Ni J. S., Ru Y., Wang S. J., Sun X. X., (2020). Experimental research on droplet drift prediction (雾滴飘移预测试验研究), *Journal of Agricultural Mechanization Research*, vol.42, no.10, pp.152-157, Nanjing/China. DOI: 10.13427/j.cnki.njyi.2020.10.026

[13] Ota K., Kasahara J. Y. L., Yamashita A., Asama H., (2022). Weed and crop detection by combining crop row detection and k-means clustering in weed infested agricultural fields, in 2022 *IEEE/SICE International Symposium on System Integration (SII)*, pp.985–990, Narvik/Norway. DOI:10.1109/SII52469.2022.9708815.

[14] Pérez-Ruíz M., Slaughter D. C., Fathallah F. A., Gliever C. J., Miller B. J., (2014). Co-robotic intra-row weed control system, *Biosystems Engineering*, vol.126, pp.45–55, Davis, CA/USA. DOI: 10.1016/j.biosystemseng.2014.07.009

[15] Ramesh K. N., Chandrika N., Omkar S. N., Meenavathi M. B., Rekha V., (2016). Detection of Rows in Agricultural Crop Images Acquired by Remote Sensing from a UAV, I.J. Image, *Graphics and Signal Processing*, vol.8, no.11, pp.25-31, Bangalore/India. DOI:10.5815/ijigsp.2016.11.04

[16] Sun B. F., Ye C., Li Y. D., Shu S. F., Cao Z. S., Wu L. F., Zhu Y., He Y., (2022). Paddy field image segmentation based on color index and threshold method (基于颜色指数与阈值法的稻田图像分割), *Journal of China Agricultural University*, vol.27, no.5, pp.86-95, Nanchang/China. DOI: 10.11841/j.issn.1007-4333.2022.05.08

[17] Tang J. L., Huang H. N., Shi L. C., Chen Z. B., Lu Y. Y., Chen H. C., (2018). An Improved Perspective Transform for Image Distortion Correction, *2018 IEEE International Conference on Consumer Electronics-Taiwan (ICCE-TW)*, pp.1-2, Taiwan/China. DOI:10.1109/ICCE-China.2018.8448538

[18] Vidovic I., Cupec R., Hocenski Z., (2016). Crop row detection by global energy minimization, *Pattern Recognition*, vol.55, pp.68–86, Croatia. DOI: http://dx.doi.org/10.1016/j.patcog.2016.01.013

[19] Wang Q., Meng Z. J., Fu W. Q., Liu H., Zhang Z. G., (2021). Multi-row crop line detection algorithm for maize seedling stage based on machine vision (基于机器视觉的玉米苗期多条作物行线检测算法), *Transactions of the Chinese Society for Agricultural Machinery,* vol.52, no.4, pp.208-213, Beijing/China. DOI: 10.6041/j.issn.1000-1298.2021.04.022

[20] Yang Z. L., Yang Y., Li C. R., Zhou Y., Zhang X. S., Yu Y., Liu D., (2022). Tasseled Crop Rows Detection Based on Micro-Region of Interest and Logarithmic Transformation, *Frontiers in Plant Science*, vol.13, Article ID 916474, Hefei/China. DOI:10.3389/fpls.2022.916474

[21] Zhai Z. Q., Zhu Z. X., Du Y. F., Song Z. H., Mao E. R., (2016). Multi-crop-row detection algorithm based on binocular vision, *Biosystems Engineering*, vol.150, pp.89-103, Beijing/China. DOI: 10.1016/j.biosystemseng.2016.08.004

[22] Zhang J. F., Wei Y. Q., Ye X. H., Liu Z. X., Qi Y. C., Maimaiti Y. S., (2025). Research Progress of Strip Compound Planting Technology of Maize and Soybean (玉米大豆带状复合种植技术研究进展), *Modern Agricultural Science and Technology*, no.11, pp.33-37, Aksu/China. DOI: 10.3969/j.issn.1007-5739.2025.11.009

[23] Zhang S., Liu Y., Xiong K., Tian Y. H., Du Y. F., Zhu Z. X., Du M. W., Zhai Z. Q., (2024). A review of vision-based crop row detection method: Focusing on field ground autonomous navigation operations, *Computers and Electronics in Agriculture*, vol.217, Article ID 109086, Beijing/China. DOI: 10.1016/j.compag.2024.109086

[24] Zhang X. Y., Wang Q. J., Wang X. H., Li H. W., He J., Lu C. Y., Yang Y., Jiang S., (2023). Automated detection of Crop-Row lines and measurement of maize width for boom spraying, *Computers and Electronics in Agriculture*, vol.211, Article ID 108406, Beijing/China. DOI: 10.1016/j.compag.2023.108406

[25] Zhao T., Noguchi S., Yang L. L., Ishii I., Chen J., (2016). Fast Edge Detection Method for Wheat Field Based on Visual Recognition (基于视觉识别的小麦收获作业线快速获取方法), *Transactions of the Chinese Society for Agricultural Machinery*, vol.47, no.11, pp.32-37, Yangling/China. DOI: 10.6041/j.issn.1000-1298.2016.11.005

[26] Zhao X. G., Ma W., Gao Y. Y., Zang Y. F., He Y. C., Wang X., (2019). Identification of early crop row for drill crops based on reverse perspective transformation (基于逆透视变换的条播作物早期作物行识别), *Journal of Jiangsu University (Natural Science Edition)*, vol.40, no.6, pp.668-675, Beijing/China. DOI: 10.3969/j.issn.1671-7775.2019.06.008

[27] Zheng K., Zhao X. G., Han C. J., He Y. K., Zhai C. Y., Zhao C. J., (2023). Design and Experiment of an Automatic Row-Oriented Spraying System Based on Machine Vision for Early-Stage Maize Corps, *Agriculture*, vol.13, Article ID 691, Beijing/China. DOI:10.3390/agriculture13060691

[28] Zhou M. C., Jiang H. Y., Bing Z. S., Su H., Knoll A., (2021). Design and evaluation of the target spray platform, *International Journal of Advanced Robotic Systems*, vol.18, pp.1-17, China. DOI:10.1177/1729881421996146